

# ClO Radical Yields in the Reaction of O(<sup>1</sup>D) with Cl<sub>2</sub>, HCl, Chloromethanes, and Chlorofluoromethanes

Karl J. Feierabend,<sup>†,‡,§</sup> Dimitrios K. Papanastasiou,<sup>†,‡</sup> and James B. Burkholder<sup>\*,†</sup>

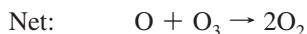
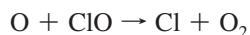
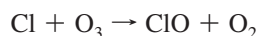
Earth System Research Laboratory, Chemical Sciences Division, National Oceanic and Atmospheric Administration, 325 Broadway, Boulder, Colorado 80305-3328, United States, and Cooperative Institute for Research in Environmental Sciences, University of Colorado, Boulder, Colorado 80309, United States

Received: August 16, 2010; Revised Manuscript Received: October 9, 2010

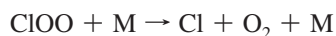
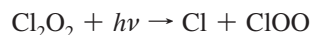
Absolute ClO radical product yields in the gas-phase reactions of O(<sup>1</sup>D) with Cl<sub>2</sub>, HCl, CCl<sub>4</sub>, CHCl<sub>3</sub>, CH<sub>2</sub>Cl<sub>2</sub>, CH<sub>3</sub>Cl, CFCl<sub>3</sub>, CF<sub>2</sub>Cl<sub>2</sub>, CF<sub>3</sub>Cl, CHFCl<sub>2</sub>, and CHF<sub>2</sub>Cl are reported. Product yields were measured using pulsed-laser photolysis of O<sub>3</sub> to produce O(<sup>1</sup>D) in the presence of excess reactant combined with dual wavelength differential cavity ring-down spectroscopic detection of the ClO radical. ClO radical absorption cross sections for the A<sup>2</sup>Π(*v* = 10) ← X<sup>2</sup>Π(*v* = 0) transition band head near 280 nm were determined between 200 and 296 K as part of this work. The ClO product yields obtained at room temperature were Cl<sub>2</sub> (0.77 ± 0.10), HCl (0.20 ± 0.04), CCl<sub>4</sub> (0.79 ± 0.04), CHCl<sub>3</sub> (0.77 ± 0.04), CH<sub>2</sub>Cl<sub>2</sub> (0.73 ± 0.04), CH<sub>3</sub>Cl (0.46 ± 0.06), CFCl<sub>3</sub> (0.79 ± 0.04), CF<sub>2</sub>Cl<sub>2</sub> (0.76 ± 0.06), CF<sub>3</sub>Cl (0.82 ± 0.06), CHFCl<sub>2</sub> (0.73 ± 0.05), and CHF<sub>2</sub>Cl (0.56 ± 0.03), where the quoted error limits are 2σ of the measurement precision. ClO product yields in the O(<sup>1</sup>D) + Cl<sub>2</sub> and CFCl<sub>3</sub> reactions were found to be independent of temperature between 200 and 296 K, within the precision of the measurements. The absolute ClO yields obtained in this study are compared with previously reported values determined using relative and indirect methods.

## 1. Introduction

The composition of Earth's stratosphere has been impacted over the last several decades by the release of anthropogenic chlorofluorocarbons (CFCs) and hydrochlorofluorocarbons (HCFCs) into the atmosphere.<sup>1</sup> These compounds are long-lived in the atmosphere and release reactive chlorine, Cl atoms, or ClO radicals, primarily in the stratosphere, following their UV photodissociation or reaction with electronically excited oxygen atoms, O(<sup>1</sup>D). The formation of reactive chlorine is particularly important in the stratosphere due to its influence on ozone abundance (e.g., the Antarctic ozone hole) through its participation in the ClO<sub>x</sub> catalytic ozone destruction cycle

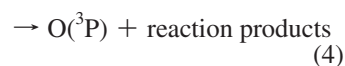
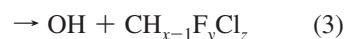
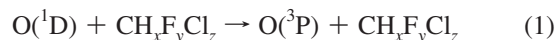


as well as the ClO dimer (Cl<sub>2</sub>O<sub>2</sub>) cycle



which plays an important role in polar stratospheric ozone chemistry. As a result, the Montreal Protocol, which phased out the production of CFCs, was adopted in 1987. Chemical processes that lead to the formation of reactive chlorine are, however, still of interest for the modeling of trends in atmospheric chemistry and ozone recovery in a changing climate.

O(<sup>1</sup>D) chemistry is particularly interesting from a kinetic and dynamics standpoint due to the potential reaction pathways available. The dynamics of the O(<sup>1</sup>D) reaction with HCl, in particular, has been studied in detail both experimentally<sup>2,3</sup> and theoretically<sup>4–6</sup> (additional references cited within). The dynamics of O(<sup>1</sup>D) reactions with polyatomic molecules has received less attention.<sup>7</sup> Rate coefficients for O(<sup>1</sup>D) reactions with the majority of atmospherically relevant chlorine containing compounds have been thoroughly studied<sup>8</sup> and approach the gas collision limit in many cases. Exothermic reaction pathways for the chlorofluoromethanes include (1) collisional (physical) quenching, (2) Cl atom abstraction to form a ClO radical, (3) H atom abstraction to form an OH radical, and (4) reactive quenching to form ground-state oxygen atoms, O(<sup>3</sup>P), and products other than the reactant, including stable and radical species.



\* Corresponding author. E-mail: James.B.Burkholder@noaa.gov.

<sup>†</sup> National Oceanic and Atmospheric Administration.

<sup>‡</sup> University of Colorado.

<sup>§</sup> Current address: The College of Wooster, Department of Chemistry, 943 College Mall, Wooster, OH 44691, U.S.

Theoretical studies<sup>4</sup> suggest that reactive pathways may proceed through O atom insertion while deactivation of O(<sup>1</sup>D) to O(<sup>3</sup>P), reaction 1, most likely occurs without insertion. Reaction product yields of O(<sup>3</sup>P), OH, CF<sub>2</sub>, and ClO have been observed in O(<sup>1</sup>D)

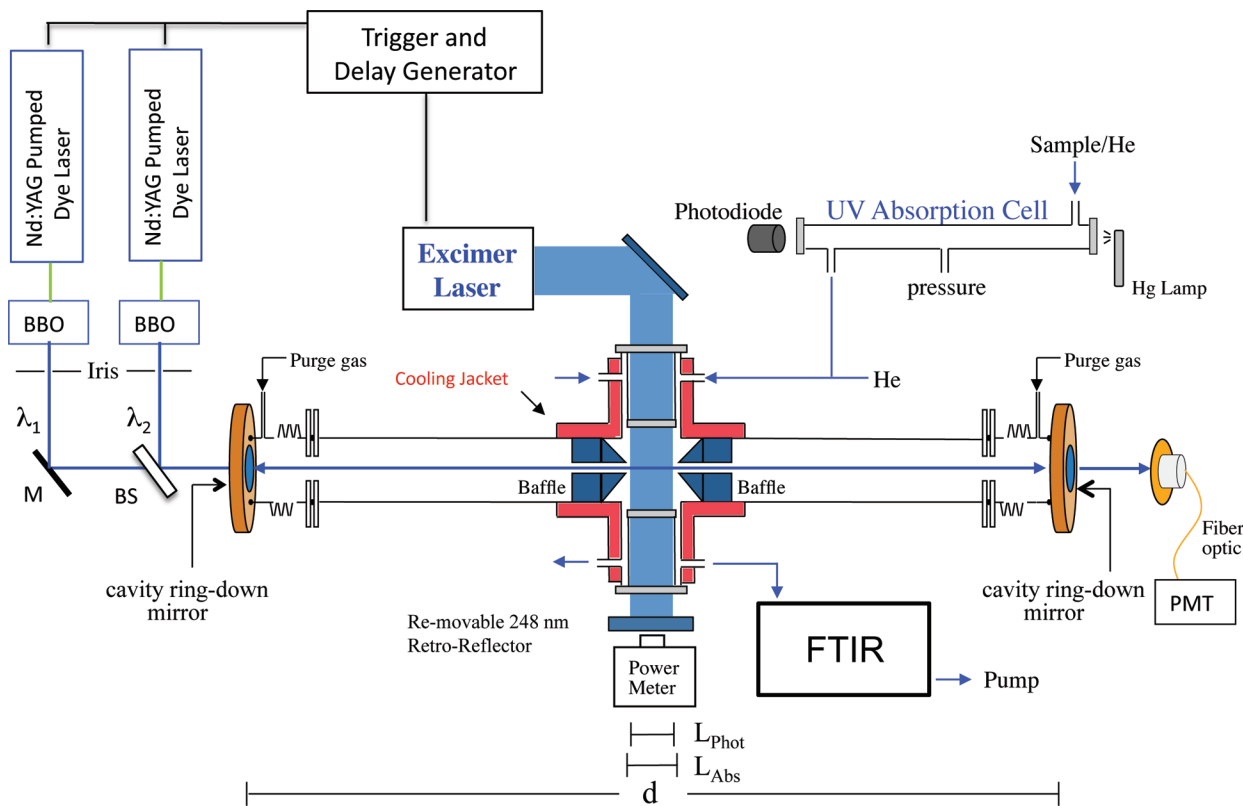


**Figure 1.** Schematic of the experimental crossed beam pulsed laser photolysis-cavity ring-down spectroscopy (PLP-CRDS) apparatus used to determine the ClO radical reaction product yields in this study: M, mirror; BS, beam splitter; PMT, photomultiplier tube; FTIR, Fourier transform infrared spectrometer;  $\lambda_1$  and  $\lambda_2$ , tunable CRDS probe wavelengths.

reactions with chloro and chlorofluoro species. In general, these studies found Cl atom abstraction to be a major reaction pathway. The uncertainty in the absolute ClO yields is, however, substantial with the most recent relative study by Takahashi et al.,<sup>9</sup> providing the most comprehensive study to date.

In this work, absolute ClO radical product yields for the reaction of O(<sup>1</sup>D) with Cl<sub>2</sub>, HCl, CCl<sub>4</sub>, CHCl<sub>3</sub>, CH<sub>2</sub>Cl<sub>2</sub>, CH<sub>3</sub>Cl, CFCl<sub>3</sub>, CF<sub>2</sub>Cl<sub>2</sub>, CF<sub>3</sub>Cl, CHFCl<sub>2</sub>, and CHF<sub>2</sub>Cl were measured. Product yields were measured over a range of pressures (50–600 Torr; He bath gas) at room temperature, while the Cl<sub>2</sub> and CFCl<sub>3</sub> reactions were also studied at lower temperatures to investigate possible changes in the reaction mechanism with temperature. The results from this work are compared with results from previous studies and lead to a reduction of the overall uncertainty in the ClO product yields for these atmospherically relevant reactions.

## 2. Experimental Details

A primary objective of this work was to measure the absolute ClO product yields in the gas-phase reaction of O(<sup>1</sup>D) with a variety of simple Cl containing species of atmospheric relevance. Cavity ring-down spectroscopy (CRDS) was used to monitor the ClO radical transient absorption signal following the production of O(<sup>1</sup>D) in the 248 nm pulsed laser photolysis of O<sub>3</sub>. A novel CRDS technique employing two independent probe beams, at wavelengths near the peak and valley of the A<sup>2</sup>Π(*v*' = 10) ← X<sup>2</sup>Π(*v*'' = 0) ClO transition band head near 280 nm, was used. The differential CRDS absorption approach improved the overall sensitivity and selectivity for detection of the ClO radical. The experimental apparatus is shown schematically in Figure 1 and consists of (1) an optical ring-down cavity, (2) a temperature regulated reactor where ClO radicals are produced

and monitored, (3) frequency doubled Nd:YAG pumped dye lasers used to generate the CRDS probe beams, (4) an excimer laser, 248 (KrF) or 351 (XeF) nm, used to initiate the gas-phase chemistry within the CRDS reactor, and (5) UV and infrared absorption measurements used to monitor the concentrations of the photolytic precursors and reactants. Details of the experimental components and methods used are described below.

Details of the cavity ring-down spectroscopy (CRDS) technique can be found elsewhere,<sup>10</sup> and only details necessary to understand the present experiments are given here. The ring-down time constant,  $\tau$ , is related to the absorption coefficient,  $\alpha(\lambda)$ , by

$$\alpha(\lambda) = [X]\sigma_X(\lambda) = \frac{1}{c} \frac{d}{L_{\text{Abs}}} \left( \frac{1}{\tau(\lambda)} - \frac{1}{\tau_0(\lambda)} \right) \quad (1)$$

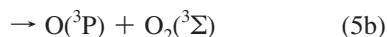
where  $\lambda$  is the probe wavelength of the CRDS measurement, X is the absorbing species,  $\sigma_X(\lambda)$  is the absorption cross section of X at wavelength  $\lambda$ ,  $d$  is the optical cavity path length,  $L_{\text{Abs}}$  is the path length for the absorbing sample,  $c$  is the speed of light, and  $\tau(\lambda)$  and  $\tau_0(\lambda)$  are the ring-down time constants with and without the absorber present, respectively. In the present experiments, the probe wavelengths were near 280 nm and the mirror reflectivity corresponded to  $\tau_0$  values of  $\sim 1.7 \mu\text{s}$  for an optical cavity length of 1 m.

The CRDS probe beams were generated from frequency doubled Nd:YAG pumped dye lasers. The probe beams entered the cavity colinearly but offset in time. The time offset was varied but was typically in the range 10–15  $\mu\text{s}$ . Light exiting the rear mirror of the optical cavity was collected with a UV

fiber optic and detected using a photomultiplier tube. The time offset allowed the first probe beam to decay to the background signal level before the second beam entered the cavity. This enabled the use of a single detector for the detection of both probe beams. Data were collected and averaged on a 16 bit waveform digitizer card at a sampling rate of 200 MHz. The air wavelengths of the probe laser beams were measured using a laser wavelength meter with an accuracy of  $\pm 0.01$  nm. The line widths of the probe lasers were  $\sim 0.1$  cm $^{-1}$ . The laser line width is sufficiently narrow compared with the vibrational–rotational structure of the ClO absorption spectrum so as not to influence the ring-down time constant and to ensure well-behaved Beer–Lambert absorption.<sup>11</sup>

Experiments were performed using a crossed pulsed laser photolysis-cavity ring-down setup, Figure 1, as used previously in this laboratory.<sup>12–15</sup> The photolysis laser beam passed the length of the reactor at a right angle to the CRD optical cavity. The temperature-regulated reactor was triple jacketed with either 248 nm AR coated or UV grade quartz windows. The stacked window configuration shown in Figure 1 prevented condensation on the window surfaces in the low temperature experiments but also enabled the inside window to extend within the temperature regulated portion of the reactor. Therefore, the gases flowing through the reactor were equilibrated to the reactor temperature before reaching the photolysis beam path. Side arms in the reactor allowed the CRDS beams to pass through the center of the reactor. Baffles mounted in the reactor side arms defined the CRDS optical path length for the absorbing species,  $L_{\text{Abs}}$ .  $L_{\text{Abs}}$  was measured geometrically and also determined experimentally using ring-down absorption at 280 nm of known concentrations of O<sub>3</sub>. The O<sub>3</sub> concentration in the gas flow was measured via UV absorption before and after the reactor. A value of  $L_{\text{Abs}} = 4.7 \pm 0.1$  cm was obtained under the typical gas flow conditions used, which was in good agreement with the geometric path length. The baffles also served to protect the ring-down mirrors from exposure to the reactive gas mixtures, provided optical baffling along the optical cavity and reduced the scattered photolysis laser light reaching the cavity mirrors. The width of the photolysis beam,  $L_{\text{Phot}}$ , filled a large fraction of the reactor width, but not the entire absorber path length,  $L_{\text{Phot}} < L_{\text{Abs}}$ . The difference in the photolysis and absorber path lengths was accounted for in the data analysis as described below. The height of the photolysis beam,  $\sim 5$  cm, was substantially larger than the CRDS probe beams, which were  $\sim 2$  mm in diameter.

O(<sup>1</sup>D) radicals were produced in the 248 nm pulsed laser photolysis of ozone



where the quantum yield for O(<sup>1</sup>D) production,  $\Phi(\text{O}(\text{}^1\text{D}))$ , is 0.9.<sup>8</sup> The photolysis laser fluence was monitored with a power meter mounted after the exit window of the reactor. The photolysis laser fluence was varied between 3 and 15 mJ cm $^{-2}$  pulse $^{-1}$  over the course of the study. The photolytic loss of O<sub>3</sub> was measured at 280 nm immediately following the photolysis pulse, 0.1  $\mu$ s delay, to determine the initial absolute O atom concentration. A short delay between the photolysis and probe laser pulses was used to minimize secondary O<sub>3</sub> loss, which was  $< 0.2\%$  under our conditions. Initial O(<sup>1</sup>D) atom concentrations were in the range  $(1\text{--}4) \times 10^{12}$  molecules cm $^{-3}$ .

**2.1. Data Analysis.** In the ozone experiments, absorption coefficients before ( $\alpha_{\text{O}_3}$ ) and after O<sub>3</sub> photolysis ( $\alpha_{\text{O}_3}^{\text{Phot}}$ ) are given by

$$\alpha_{\text{O}_3} = \frac{d}{cL_{\text{Abs}}} \left( \frac{1}{\tau_{\text{O}_3}} - \frac{1}{\tau_0} \right) = [\text{O}_3]_0 \sigma_{\text{O}_3}(280 \text{ nm}) \quad (\text{II})$$

and

$$\alpha_{\text{O}_3}^{\text{Phot}} = \frac{d}{cL_{\text{Abs}}} \left( \frac{1}{\tau_{\text{Phot}}} - \frac{1}{\tau_0} \right) = [\text{O}_3]_0 \sigma_{\text{O}_3}(280 \text{ nm}) \times \left( 1 - \frac{L_{\text{Phot}}}{L_{\text{Abs}}} F \sigma_{\text{O}_3}(248 \text{ nm}) \right) \quad (\text{III})$$

where  $L_{\text{Abs}}$  and  $L_{\text{Phot}}$  are the absorption and photolysis path lengths, respectively,  $\tau_{\text{O}_3}$  is the ring-down time constant with O<sub>3</sub> in the reactor,  $\sigma_{\text{O}_3}(\lambda)$  is the ozone absorption cross section at wavelength  $\lambda$  (the ring-down ( $\sim 280$  nm) and photolysis (248 nm) wavelengths),  $\tau_{\text{Phot}}$  is the ring-down time constant with the measurement initiated 0.1  $\mu$ s after the photolysis laser pulse, and  $F$  is the photolysis laser fluence. The quantum yield for ozone photolysis at 248 nm is unity.<sup>8</sup> Subtracting (III) from (II) and rearranging yields

$$\begin{aligned} \Delta\alpha_{\text{O}_3} &= \frac{d}{cL_{\text{Abs}}} \left( \frac{1}{\tau_{\text{O}_3}} - \frac{1}{\tau_{\text{Phot}}} \right) = \frac{L_{\text{Phot}}}{L_{\text{Abs}}} \sigma_{\text{O}_3}(280 \text{ nm}) [\text{O}_3]_0 F \sigma_{\text{O}_3}(248 \text{ nm}) \\ &= \frac{L_{\text{Phot}}}{L_{\text{Abs}}} \sigma_{\text{O}_3}(280 \text{ nm}) [\text{O}(\text{}^1\text{D})]_0 \frac{1}{\Phi(\text{O}(\text{}^1\text{D}))} \end{aligned} \quad (\text{IV})$$

That is, the difference in the absorption coefficients,  $\Delta\alpha_{\text{O}_3} = \alpha_{\text{O}_3} - \alpha_{\text{O}_3}^{\text{Phot}}$ , is directly proportional to the initial O(<sup>1</sup>D) concentration,  $[\text{O}(\text{}^1\text{D})]_0$ . Equation IV applies for both probe wavelengths in the ozone photolysis experiments. With a reactant present in the reactor, ClO radicals are produced and the differential absorption coefficient,  $\alpha_{\text{ClO}}^{\text{d}}$ , measured at a given delay time following the photolysis pulse (typically 10  $\mu$ s) is given by

$$\alpha_{\text{ClO}}^{\text{d}} = \frac{d}{cL_{\text{Abs}}} \left( \left( \frac{1}{\tau_{\text{Phot}}} - \frac{1}{\tau_0/\lambda_1} \right) - \left( \frac{1}{\tau_{\text{Phot}}} - \frac{1}{\tau_0/\lambda_2} \right) \right) = \frac{L_{\text{Phot}}}{L_{\text{Abs}}} [\text{ClO}] \Delta\sigma_{\text{ClO}}(T) \quad (\text{V})$$

where  $\lambda_1$  and  $\lambda_2$  are the peak and valley probe wavelengths, respectively, and  $\Delta\sigma_{\text{ClO}}(T)$  is the difference in the ClO absorption cross section between these wavelengths,  $\Delta\sigma_{\text{ClO}}(T) = \sigma_{\text{ClO}}^{\text{Peak}}(T) - \sigma_{\text{ClO}}^{\text{Valley}}(T)$  at temperature  $T$ . That is, the differential absorption coefficient is directly proportional to the ClO radical concentration produced in the O(<sup>1</sup>D) reaction with the reactant. The probe laser wavelengths were set to near the peak and valley of the 10–0 transition band head at 279.67 and 279.56 nm, respectively. Using pairs of measured values for the ozone loss and ClO radical production, an analysis of the linear relationship

$$\left( \frac{1}{\tau_{\text{O}_3}} - \frac{1}{\tau_{\text{Phot}}} \right) \quad \text{versus} \quad \left( \left( \frac{1}{\tau_{\text{Phot}}} - \frac{1}{\tau_0/\lambda_1} \right) - \left( \frac{1}{\tau_{\text{Phot}}} - \frac{1}{\tau_0/\lambda_2} \right) \right) \quad (\text{VI})$$

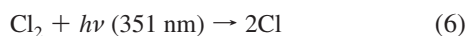
yields

$$\text{slope} = \frac{[\text{ClO}]\Phi(\text{O}^1\text{D})}{[\text{O}^1\text{D}]_0} \frac{\Delta\sigma_{\text{ClO}}(T)}{\sigma_{\text{O}_3}(280 \text{ nm})} = \frac{Y_{\text{ClO}}\Phi(\text{O}^1\text{D}) \Delta\sigma_{\text{ClO}}(T)}{\sigma_{\text{O}_3}(280 \text{ nm})} \quad (\text{VII})$$

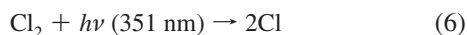
The measured slope was used to determine  $Y_{\text{ClO}}\Delta\sigma_{\text{ClO}}(T)$  where  $Y_{\text{ClO}}$  is the ClO radical yield in the O(<sup>1</sup>D) + reactant reaction. ClO product yields for each of the molecules included in this study were determined from a least-squares fit of the experimental data obtained using various initial ozone concentrations and photolysis laser fluences to eq VII. Typically, three different photolysis laser fluences were used for each ozone concentration, and at least three different ozone concentrations were used. Small corrections were applied to the experimentally measured values to account for the differential cross section of ozone and measured variations in the photolysis laser fluence and the initial ozone concentration that are not included in the equations presented above. In the Cl<sub>2</sub> and HCl reaction systems, a minor correction, <10%, was applied to account for secondary chemistry that produced ClO on the time scale of the ring-down measurements, ~5 μs, which was verified using measured temporal profiles.

**2.2. ClO Radical Cross Section.** Three independent photolytic systems were used in the determination of the ClO differential absorption cross section,  $\Delta\sigma_{\text{ClO}}(T)$ .

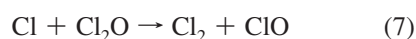
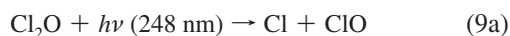
Source 1:



Source 2:



Source 3:



where  $k_7(298 \text{ K}) = 9.6 \times 10^{-11} \text{ cm}^3 \text{ molecule}^{-1} \text{ s}^{-1}$ ,  $k_8(298 \text{ K}) = 1.2 \times 10^{-11} \text{ cm}^3 \text{ molecule}^{-1} \text{ s}^{-1}$ ,  $k_{10}(298 \text{ K}) = 2.9 \times 10^{-12} \text{ cm}^3 \text{ molecule}^{-1} \text{ s}^{-1}$ , and ClO radical product channels are the only channels formed in reactions 7, 8, and 10.<sup>8</sup> The major product channel in the 248 nm photolysis of Cl<sub>2</sub>O is (9a), although a recent study by Zou et al.<sup>16</sup> found the three atom product channel branching ratio to be ~15%. Recent work in our laboratory found the O atom quantum yield to be ~20%. To quantify the ClO radical production in source 3, the photolysis laser fluence was determined in separate experiments in which O<sub>3</sub> was photolyzed and its loss measured by CRDS. The temperature dependence of the ClO absorption cross section

was determined using sources 2 and 3. The Cl<sub>2</sub>O and O<sub>3</sub> concentrations were in the range  $(0.11\text{--}3.4) \times 10^{15}$  and  $(0.08\text{--}6.2) \times 10^{14} \text{ molecules cm}^{-3}$ , respectively.

The ClO absorption spectrum was measured in this study over a narrow wavelength range, 279–285.5 nm, using the dual wavelength CRDS technique by holding one probe laser at a fixed wavelength, as a reference, and stepping the wavelength of the second laser in increments of 0.005 nm. ClO radicals were produced by the 248 nm photolysis of Cl<sub>2</sub>O while using a cylindrical lens mounted in front of the reactor entrance window to partially focus the photolysis beam and increase the photolysis laser fluence, thereby increasing the ClO absorption signal. Note that the lens was not used in the quantitative ClO product yield determinations due to nonuniformity of the photolysis beam. The absorption coefficient was recorded after a 150 μs delay between the photolysis and probe lasers to ensure the completion of the secondary source chemistry. The Cl<sub>2</sub>O precursor contribution to the spectrum was accounted for independently using the measured absorption of Cl<sub>2</sub>O at each wavelength interval (photolysis laser off) and then subtracting the appropriate fraction of this absorption from the total signal. The ClO spectrum was recorded over narrow spectral windows and constructed using overlapping spectral regions. The ClO spectrum was recorded at 200 and 298 K and used to confirm the ClO radical measurement itself and help establish the absolute ClO absorption cross sections and their temperature dependence needed for the absolute ClO product yield determinations.

**2.3. Materials.** He (UHP, 99.999%), N<sub>2</sub> (UHP, 99.99%), SF<sub>6</sub> (99.999%), and O<sub>2</sub> (UHP, 99.99%) were used as supplied. Cl<sub>2</sub> (UHP, 99.97%), HCl (>99%), CCl<sub>4</sub> (99.9%, CHROMASOLV grade), CHCl<sub>3</sub> (99.9%, CHROMASOLV grade), CH<sub>2</sub>Cl<sub>2</sub> (>99%), CH<sub>3</sub>Cl (>99.5%), CFCl<sub>3</sub> (>99.7%), CF<sub>2</sub>Cl<sub>2</sub> (>99%), CF<sub>3</sub>Cl (>99%), CHFCl<sub>2</sub> (>99%), and CHF<sub>2</sub>Cl (>99%) were used as supplied. Liquid samples of CCl<sub>4</sub> and CHCl<sub>3</sub> were degassed using freeze–pump–thaw cycles prior to use and stored under vacuum in Pyrex reservoirs with Teflon stopcocks.

Ozone was prepared by passing O<sub>2</sub> through an ozonizer and stored on silica gel at 195 K. A flow of He through the ozone silica gel trap was used to introduce ozone into the gas flow through the apparatus. The O<sub>3</sub> concentration was measured online at 298 K using UV absorption cells either before or after the CRD reactor or in situ at the temperature of the reactor using CRDS at ~280 nm. The online UV absorption measurements were made using a 253.7 nm Hg pen-ray lamp light source combined with a narrow bandpass filter and a photodiode detector. O<sub>3</sub> absorption cross sections and their temperature dependence were taken from Sander et al.<sup>8</sup> The absorption cells were made from 1 in. diameter Pyrex tubing fitted with quartz windows. Absorption cells with path lengths of 50 and 100 cm were used during the course of the experiment. The O<sub>3</sub> concentrations measured before, in, and after the reactor were in good agreement, within 2% after accounting for differences in pressure and temperature, under all experimental conditions.

An accurate measurement of the reactant concentration is not required in the ClO product yield determination provided that it is sufficiently high to scavenge all O(<sup>1</sup>D) radicals produced in the O<sub>3</sub> photolysis. The reactant concentrations were varied during the experiments to test for systematic errors in the measurement but were typically >2 × 10<sup>16</sup> molecules cm<sup>-3</sup>. Reactant concentrations were measured using infrared absorption spectroscopy, except for Cl<sub>2</sub> and CHFCl<sub>2</sub> as described below. Infrared absorption spectra were recorded between 500 and 4000 cm<sup>-1</sup> using a Fourier transform spectrometer at a spectral

resolution of  $1\text{ cm}^{-1}$  in 50 coadded scans. The spectrometer was typically situated after the photochemical reactor. An absorption cell (15 cm optical path length,  $74\text{ cm}^3$  total volume, KBr windows) was used for all infrared measurements. Absorption cross sections and infrared band strengths used in this study were taken from the literature.<sup>17–21</sup> The precursor concentrations in the reactor were calculated from the absorption measurements and included correction factors to account for sample dilution and differences in pressure and temperature between the absorption cells and the CRDS reactor. The concentrations of  $\text{Cl}_2$  and  $\text{CHFCl}_2$  were determined using measured flow rates and pressures. The concentration of  $\text{Cl}_2$  was also monitored using absorption at  $\sim 280\text{ nm}$  from the cavity ring-down absorption measurements. Reactants were added directly to the gas flow from the source cylinders. For the liquid samples the reactant was introduced into the gas flow by passing a flow of bath gas over the liquid surface prior to dilution with the main gas flow and entering the reactor. The sample reservoirs were kept in constant temperature baths to help stabilize the sample flow out of the reservoir.

Dichlorine oxide ( $\text{Cl}_2\text{O}$ ) was prepared by oxidizing  $\text{Cl}_2$  with  $\text{HgO}$ . A flow of  $\text{Cl}_2$  gas passed through a reactor containing glass beads coated with dry  $\text{HgO}$ . The gas stream exiting the reactor contained  $\text{Cl}_2\text{O}$  and  $\text{Cl}_2$  and was condensed at 195 K. The  $\text{Cl}_2\text{O}$  samples were purified by trap-to-trap distillation to remove the  $\text{Cl}_2$  impurity. The  $\text{Cl}_2\text{O}$  purity,  $>99\%$ , was measured by UV absorption.  $\text{Cl}_2\text{O}$  was added to the apparatus by passing a small flow of bath gas over the liquid sample held in a Pyrex reservoir at 195 K. The  $\text{Cl}_2\text{O}$  concentration was measured in situ using UV absorption by CRDS and online by UV absorption using a 253.7 nm Hg pen-ray lamp light source; the concentration measurements agreed to within 2% under all experimental conditions.

The total gas flow rate through the reactor was typically 2500 sccm. To ensure that a fresh sample was present for each photolysis laser pulse, experiments were performed with a laser repetition rate of  $<3\text{ Hz}$ . Gas flow rates were measured using calibrated electronic mass flow transducers. Pressures were measured using 100 and 1000 Torr capacitance manometers.

### 3. Results and Discussion

Figure 2 shows the UV absorption spectrum of the ClO radical measured between 279.2 and 285 nm at 200 and 298 K. The spectra were recorded using source 3 with  $\sim 3 \times 10^{15}$  molecules  $\text{cm}^{-3}$   $\text{Cl}_2\text{O}$  in 100 Torr  $\text{N}_2$  bath gas as the ClO radical source and an estimated photolysis laser fluence of  $\sim 130\text{ mJ cm}^{-2}\text{ pulse}^{-1}$  (focused beam). Several features clearly stand out in the spectra. The ClO spectrum shows a strong temperature dependence and a high degree of rotational structure, which is resolved to the transition line width; line widths for the 9–0 and 10–0 bands are 4.92 and  $5.79\text{ cm}^{-1}$ , respectively.<sup>22</sup> Transitions from the 1/2 and 3/2 spin states of the ClO radical, spin splitting of  $318\text{ cm}^{-1}$ , are clearly visible in the spectra, and the intensity of the 1/2 spin-state transitions decrease with decreasing temperature, as expected. Transitions for both  $^{35}\text{ClO}$  and  $^{37}\text{ClO}$  isotopes are also observed in the spectrum. The sharp 10–0 band head is well suited for the detection of ClO using the dual wavelength CRDS approach. The band head has an increasing differential absorption cross section with decreasing temperature. The measured spectra are in good agreement with synthetic spectra, also shown in Figure 2, calculated using Boltzmann distributions in the ground electronic state and available dipole transition moments, spectroscopic parameters, and transition line widths for the 9–0 and 10–0 bands from

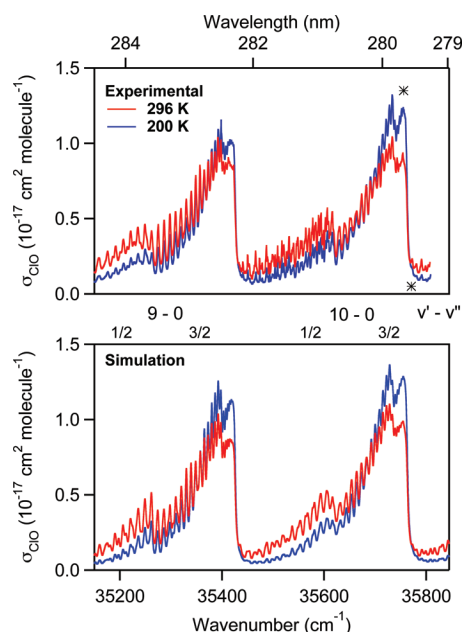


**Figure 2.** UV absorption spectrum of the ClO radical measured in this work over the wavelength region 279–285 nm at 296 and 200 K using cavity ring-down spectroscopy (upper) and calculated using spectroscopic parameters from the literature (lower). The absorption spectrum includes the  $\text{A}^2\Pi(v'' = 9) \leftarrow \text{X}^2\Pi(v' = 0)$  and  $\text{A}^2\Pi(v'' = 10) \leftarrow \text{X}^2\Pi(v' = 0)$  transitions for the  $^{35}\text{ClO}$  and  $^{37}\text{ClO}$  isotopes and ClO 1/2 and 3/2 spin states. The \* indicates the wavelengths for the peak and valley CRDS probe lasers used in this study.

previous spectroscopic studies.<sup>22,23</sup> Some systematic differences are, however, observed in the structure and line widths of the weaker transitions near 280.8 nm.

**3.1. ClO Absorption Cross Section Determination.** The absolute differential ClO absorption cross section and its temperature dependence,  $\Delta\sigma_{\text{ClO}}(T)$ , was determined using the source chemistry described in the experimental section. Figures 3 and 4 show representative experimental data used in the determination of  $\Delta\sigma_{\text{ClO}}(T)$ . Figure 3 shows pairs of differential and valley absorption coefficients measured following the 351 nm photolysis of  $\text{Cl}_2$  in the presence of  $\text{Cl}_2\text{O}$  and  $\text{O}_3$ . The interpretation of these measurements is straightforward as the only chemistry occurring within the first 100  $\mu\text{s}$  following the photolysis pulse is the reaction of the Cl atoms with  $\text{Cl}_2\text{O}$  or  $\text{O}_3$ , reactions 7 and 8, respectively. The differential signal is zero at time zero; i.e., there is no initial ClO radical production. However, the initial absorption coefficient at each probe wavelength is high due to absorption by the  $\text{Cl}_2\text{O}$  and  $\text{O}_3$  reactants;  $\text{Cl}_2\text{O}$  and  $\text{O}_3$  absorption limited the range of their initial concentrations used in these experiments. It is clear from the valley absorption coefficients that the absorption cross section of ClO at 279.56 nm is greater than that of  $\text{Cl}_2\text{O}$ ,  $\sigma_{\text{ClO}}^{\text{valley}}(296\text{ K}) > 1.2 \times 10^{-18}\text{ cm}^2\text{ molecule}^{-1}$ , because  $\alpha(279.56\text{ nm})$  increases following photolysis.  $\sigma_{\text{ClO}}^{\text{valley}}(296\text{ K})$  is also less than the cross section of  $\text{O}_3$ ,  $4.7 \times 10^{-18}\text{ cm}^2\text{ molecule}^{-1}$ , because  $\alpha(279.56\text{ nm})$  decreases after photolysis in the  $\text{O}_3$  experiments. In the  $\text{O}_3$  experiments, the valley measurements are relatively insensitive to the ClO absorption cross section value and provide a reasonably accurate measure of the  $\text{O}_3$  loss and thus the ClO radical production. Simulations of the reaction chemistry and measured absorption temporal profiles, while treating  $\Delta\sigma_{\text{ClO}}(296\text{ K})$  and  $\sigma_{\text{ClO}}^{\text{valley}}(296\text{ K})$  as variable parameters, were used to obtain optimized room temperature ClO cross sections of  $(7.5 \pm 0.75) \times 10^{-18}$  and  $(1.85 \pm 0.4) \times 10^{-18}\text{ cm}^2\text{ molecule}^{-1}$ , respectively. The optimized simulations are included

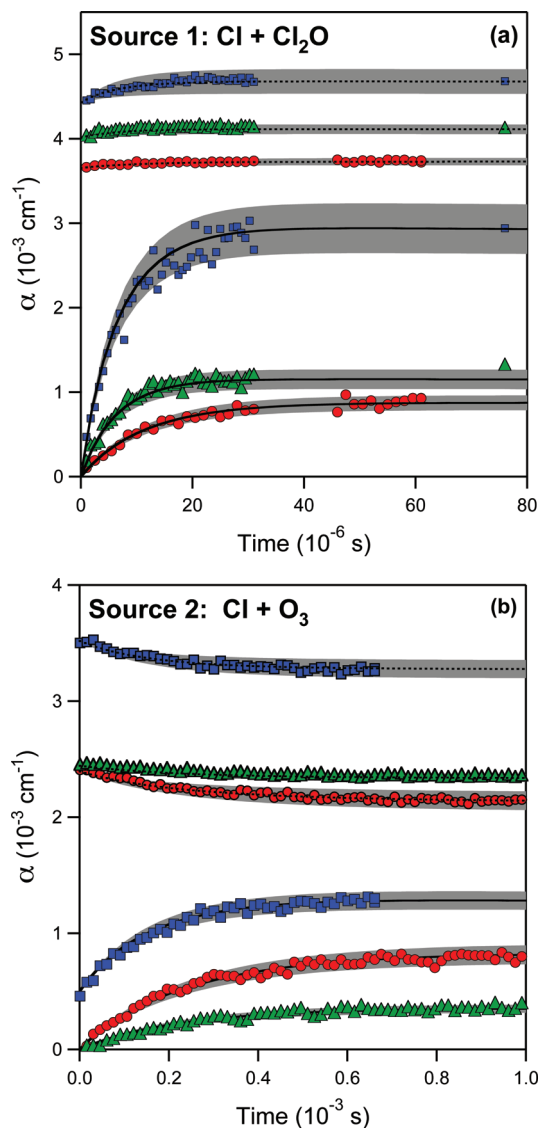


**Figure 3.** Representative ClO absorption coefficient,  $\alpha$ , temporal profiles at 296 K for the ClO radical sources 1 (a) and 2 (b) measured at the valley wavelength (279.56 nm) (three profiles at the top of the figures), and the differential signal,  $\alpha_{\text{ClO}}^{\text{d}}$  (three profiles at the bottom of the figures). Experimental conditions for (a), displayed as circles, triangles, and squares, respectively: initial  $[\text{Cl}_2\text{O}] = 0.95, 1.7, 1.7$  ( $10^{15}$  molecules  $\text{cm}^{-3}$ );  $[\text{Cl}_2] = 1.95, 3.7, 5.34$  ( $10^{16}$  molecules  $\text{cm}^{-3}$ ); photolysis laser fluence, 30, 21, 37  $\text{mJ cm}^{-2} \text{pulse}^{-1}$ . The  $\alpha$  profiles measured at the ClO valley wavelength have been offset by +0.001, +0.002, and +0.001, respectively, for clarity. Experimental conditions for (b), displayed as circles, triangles, and squares, respectively: initial  $[\text{O}_3] = 3.74, 3.84, \text{and } 5.68$  ( $10^{14}$  molecules  $\text{cm}^{-3}$ );  $[\text{Cl}_2] = 3.4, 3.4, \text{and } 4.7$  ( $10^{16}$  molecules  $\text{cm}^{-3}$ ); photolysis laser fluence, 17, 7, and 11.5  $\text{mJ cm}^{-2} \text{pulse}^{-1}$ .  $\alpha_{\text{ClO}}^{\text{d}}$  (squares) has been offset by +0.0005 for clarity. The solid and dotted lines are simulations (see text for details) of the measured temporal profiles obtained with  $\Delta\sigma_{\text{ClO}}(296 \text{ K}) = 7.5 \times 10^{-18} \text{ cm}^2 \text{ molecule}^{-1}$  and  $\sigma_{\text{ClO}}^{\text{Valley}}(296 \text{ K}) = 1.85 \times 10^{-18} \text{ cm}^2 \text{ molecule}^{-1}$ . The extremes of the gray shaded regions were calculated with  $\pm 10\%$  of the optimized  $\Delta\sigma_{\text{ClO}}(296 \text{ K})$  value and  $\pm 20\%$  and  $\pm 40\%$  for  $\sigma_{\text{ClO}}^{\text{Valley}}(296 \text{ K})$  for sources 1 and 2, respectively.

in Figures 3 and 4. Also shown in Figures 3 and 4, as the shaded regions, are simulations in which  $\Delta\sigma_{\text{ClO}}(296 \text{ K})$  and  $\sigma_{\text{ClO}}^{\text{Valley}}(296 \text{ K})$  were increased and decreased by 10% and 20 (or 40)%, respectively. This range of ClO cross section values covers the overall spread in the measured absorption coefficients obtained in all experiments performed over a range of experimental conditions. Source 2 was also used to measure  $\Delta\sigma_{\text{ClO}}(200 \text{ K})$

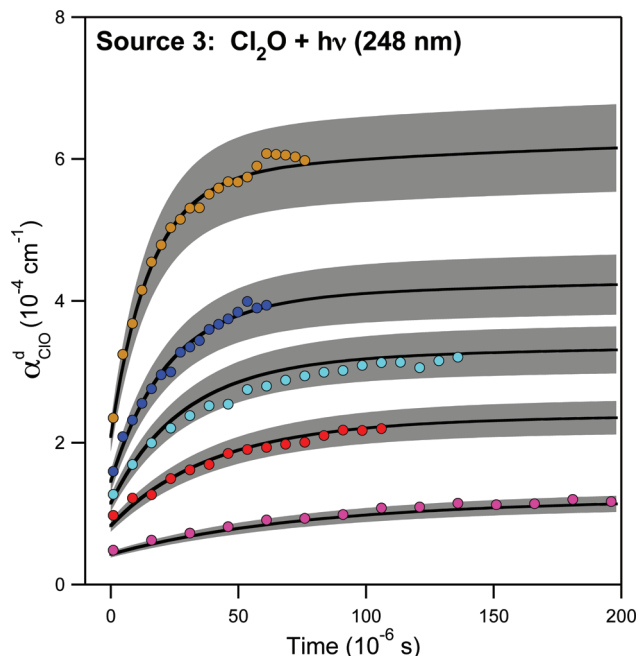
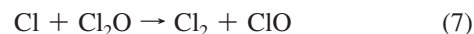


**Figure 4.** ClO absorption coefficient,  $\alpha_{\text{ClO}}^{\text{d}}$ , temporal profiles measured at 296 K following the 248 nm pulsed laser photolysis of  $\text{Cl}_2\text{O}$ , source 3. Measurements were made with 300 Torr  $\text{N}_2$  and a photolysis laser fluence of  $\sim 23 \text{ mJ cm}^{-2} \text{pulse}^{-1}$  with initial  $\text{Cl}_2\text{O}$  concentrations of 1.46, 2.8, 3.95, 5.0, and 7.2 in units of  $10^{14}$  molecules  $\text{cm}^{-3}$  (from bottom to top of the figure). The lines are simulations of the photochemical system (see text for details) with  $\Delta\sigma_{\text{ClO}}(296 \text{ K}) = 7.5 \times 10^{-18} \text{ cm}^2 \text{ molecule}^{-1}$ . The extremes of the gray shaded regions were calculated with  $\Delta\sigma_{\text{ClO}}(296 \text{ K})$  values  $\pm 10\%$  of this value.

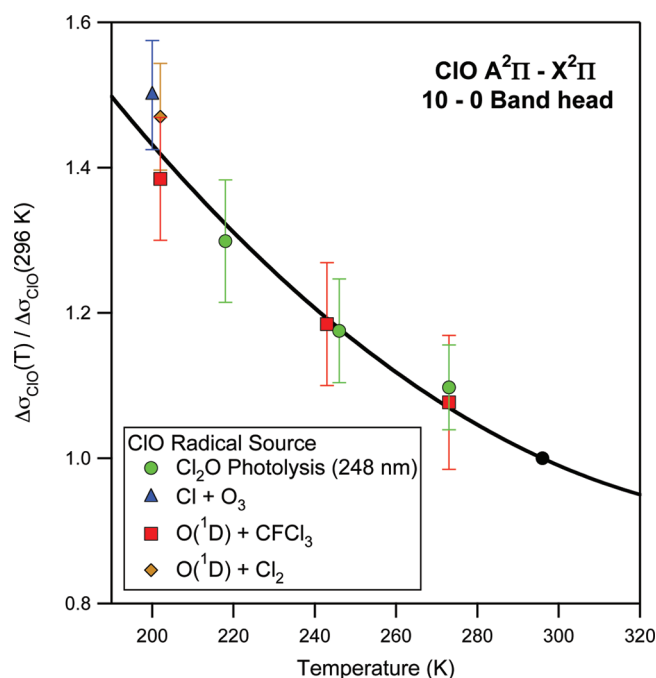
$= (10.9 \pm 1.0) \times 10^{-18} \text{ cm}^2 \text{ molecule}^{-1}$ , a value 45% greater than the room temperature cross section value.

Figure 4 shows several representative  $\Delta\sigma_{\text{ClO}}(296 \text{ K})$  temporal profiles obtained using the 248 nm pulsed laser photolysis of  $\text{Cl}_2\text{O}$  as the ClO radical source. The initial jump in the absorption coefficient at time zero is due to ClO radicals produced as a primary photolysis product, reaction 9a. A systematic dependence of the initial ClO absorption signal on the total system pressure was observed at pressures  $< 100$  Torr, presumably due to the formation of excited ClO radicals in reaction 9; our measurements only monitor transitions from the ClO ground vibrational state.  $\text{Cl}_2\text{O}$  photolysis experiments were performed over a range of pressures using different bath gases (He,  $\text{N}_2$ , and  $\text{SF}_6$ ). The initial ClO photolysis signal was found to be independent of pressure for pressures  $> 300$  Torr, which is consistent with collisional relaxation of nascent vibrationally excited ClO radicals. All quantitative experiments using the  $\text{Cl}_2\text{O}$  photolysis source were, therefore, performed at total pressures  $> 300$  Torr. The subsequent rise in  $\Delta\sigma_{\text{ClO}}(296 \text{ K})$  over the next 100–200  $\mu\text{s}$  is due to secondary reactions of the photolysis products, Cl and O atoms, with  $\text{Cl}_2\text{O}$  to produce additional ClO radicals



The initial ClO concentration,  $[\text{ClO}]_0$ , was determined using

$$[\text{ClO}]_0 = \sigma_{\text{Cl}_2\text{O}}(248 \text{ nm})[\text{Cl}_2\text{O}]F\Phi(\text{ClO}) \quad (\text{VIII})$$



**Figure 5.** Relative temperature dependence of the ClO radical differential absorption cross section,  $\Delta\sigma_{\text{ClO}}(T)$ , for the  $\text{A}^2\Pi(v' = 10) \leftarrow \text{X}^2\Pi(v'' = 0)$  band head measured in this work using various ClO radical sources as indicated in the legend. The error bars shown were taken from the  $2\sigma$  precision of the measurements. The line is a least-squares fit to the simulated spectrum temperature dependence,  $\Delta\sigma_{\text{ClO}}(T)/\Delta\sigma_{\text{ClO}}(296 \text{ K}) = 3.5234 - 0.014486T + 2.0137 \times 10^{-5}T^2$ , which is visually indistinguishable from a fit of the experimental data.

where  $\Phi(\text{ClO})$  is the ClO quantum yield in  $\text{Cl}_2\text{O}$  photolysis at 248 nm. The photolysis laser fluence,  $F$ , was determined separately under identical conditions either before or after the  $\text{Cl}_2\text{O}$  photolysis experiment. The laser fluence was measured using 248 nm photolysis of  $\text{O}_3$  and the measured loss of  $\text{O}_3$  at 280 nm. The lines in Figure 4 are simulations of the ClO temporal profile using the calibrated photolysis laser fluence and secondary chemistry where  $\Delta\sigma_{\text{ClO}}(296 \text{ K})$  was treated as a variable parameter. The simulation of this data set and others obtained over a range of initial  $\text{Cl}_2\text{O}$  concentrations and photolysis laser fluences yielded  $\Delta\sigma_{\text{ClO}}(296 \text{ K}) = (7.5 \pm 0.75) \times 10^{-18} \text{ cm}^2 \text{ molecule}^{-1}$  where the error limits are at the  $2\sigma$  level and include estimated systematic errors. The extremes of the shaded regions shown in Figure 4 are ClO temporal profile simulation results obtained using the high and low limits of  $\Delta\sigma_{\text{ClO}}(296 \text{ K})$ . The range of uncertainty in  $\Delta\sigma_{\text{ClO}}(296 \text{ K})$  incorporates the full range of the experimental data obtained in all experiments performed over a range of initial conditions.

ClO cross section experiments were also performed using source 3 at 273, 243, and 218 K. The differential ClO absorption cross section increased with decreasing temperature with values of  $\Delta\sigma_{\text{ClO}}(273 \text{ K}) = (8.23 \pm 0.45) \times 10^{-18} \text{ cm}^2 \text{ molecule}^{-1}$ ,  $\Delta\sigma_{\text{ClO}}(243 \text{ K}) = (8.81 \pm 0.53) \times 10^{-18} \text{ cm}^2 \text{ molecule}^{-1}$ , and  $\Delta\sigma_{\text{ClO}}(218 \text{ K}) = (9.74 \pm 0.63) \times 10^{-18} \text{ cm}^2 \text{ molecule}^{-1}$  where the estimated uncertainties are at the  $2\sigma$  level. A summary of the ClO cross section temperature dependence results is shown in Figure 5. A simulation of the relative temperature dependence of the ClO cross section, similar to the spectra shown in Figure 2, over the range 190–320 K using available spectroscopic parameters was in excellent agreement with the experimental data as shown in Figure 5. An empirical polynomial fit of simulated ClO differential cross section temperature dependence yields

$$\Delta\sigma_{\text{ClO}}(T)/\Delta\sigma_{\text{ClO}}(296 \text{ K}) = 3.5234 - 0.014486T + 2.0137 \times 10^{-5}T^2 \quad (\text{IX})$$

where temperature is in Kelvin (K). The fit reproduces the simulation results very well, to better than 1% over the entire temperature range, and is visually indistinguishable from a least-squares fit of the experimental data.

**3.2. ClO Product Yield Determination.** A representative sequence of experimental measurements used in the determination of the ClO product yield in the  $\text{O}(^1\text{D}) + \text{CFCl}_3$  reaction at 296 K and 300 Torr He is shown in Figure 6. Figure 6 highlights the various measurement steps in a typical ClO yield determination experiment (using both probe lasers). First,  $\tau_0$  was measured with bath gas flowing through the reactor (top panel). Next, laser fluence calibration measurements were made with  $\text{O}_3$  added to the reactor (middle panel). Steps 2 and 6 are measurements of the  $\text{O}_3$  concentration, i.e., in the absence of photolysis, and confirm the stability of the  $\text{O}_3$  concentration over the course of the experiment. Steps 3–5 are made using three different photolysis laser fluences. Finally, reactant was added to the gas mixture ( $\text{CFCl}_3$  in this example) and steps 2–6 were repeated. Average ring-down time constants obtained over the duration of the various steps were used in the data analysis. The data shown in Figure 6 are representative of the precision of the time constant measurements made for the other reactants included in this study.

$\text{O}(^1\text{D})$  reactions with chlorinated compounds are known to produce vibrationally excited ClO radicals.<sup>7</sup> For  $\text{CCl}_4$  and chlorofluoromethanes the extent of ClO radical vibrational excitation was found previously<sup>7</sup> to increase with the increasing reaction exothermicity,  $\Delta_r H^0$ , which are between  $-22$  and  $-45 \text{ kcal mol}^{-1}$  for the chloromethanes and chlorofluoromethanes included in the present study. The presence of vibrationally excited ClO would lead to a systematic underestimate of the ClO reaction product yield in our experiments, as we only observed  $\text{ClO}(v = 0)$ . Experiments performed over a range of pressures with He and  $\text{SF}_6$  bath gases found that the ClO yields obtained at system pressures  $>300$  Torr were independent of pressure. All quantitative ClO yield experiments reported here were performed at pressures between 300 and 600 Torr total pressure.

Figure 7 shows a summary of the experimental data for the  $\text{O}(^1\text{D}) + \text{CFCl}_3$  reaction obtained at 202, 243, 273, and 296 K. The experimental data follow a linear relationship with increasing slope with decreasing temperature between the measured absorption coefficients for the formation of ClO and photolytic loss of  $\text{O}_3$ , eq VII. The data shown in Figure 7 are a compilation of the data obtained over a range of reactant concentrations and photolysis laser fluences. Summary figures for the other compounds included in this study are provided in the Supporting Information. A linear least-squares fit of the data shown in Figure 7, at each temperature, yields  $Y_{\text{ClO}}\Delta\sigma_{\text{ClO}}(T)$ , using eq VII. The increase in  $Y_{\text{ClO}}\Delta\sigma_{\text{ClO}}(T)$  with decreasing temperature can be fully accounted for by the temperature dependence of the ClO differential absorption cross section,  $\Delta\sigma_{\text{ClO}}(T)$ , given earlier and shown in Figure 5. That is, the ClO product yield was found to be independent of temperature within the precision of the measurements. This is further illustrated in Figure 5 where the relative change in  $\Delta\sigma_{\text{ClO}}(T)$  as a function of temperature obtained from the  $\text{O}(^1\text{D}) + \text{CFCl}_3$  and  $\text{O}(^1\text{D}) + \text{Cl}_2$  experiments are plotted assuming a temperature independent ClO product yield. Excellent agreement between the yield measurements and those obtained in our cross section determination experiments described above is observed. These comparisons provide a self-

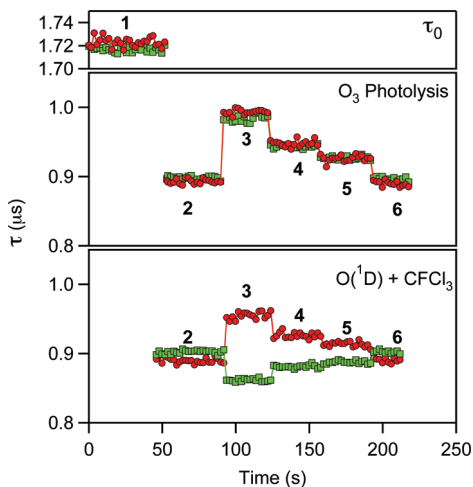


**Figure 6.** Representative sequence of experimental measurements in the determination of the ClO product yield in the O(<sup>1</sup>D) + CFCl<sub>3</sub> reaction at 296 K in 300 Torr He; CRDS probes at 279.67 nm (ClO peak, green squares) and 279.56 nm (ClO valley, red circles). The top panel shows  $\tau_0$  where only bath gas was flowing through the reactor. The center panel shows a sequence of measurements made with O<sub>3</sub> added to the cell with different photolysis laser fluences. Sections 2 and 6 were with no photolysis laser. Measurements with the reactant added to the gas flow (bottom panel) were made under conditions identical to those for the middle panel, but with a 10  $\mu$ s delay between the photolysis and probe pulses.

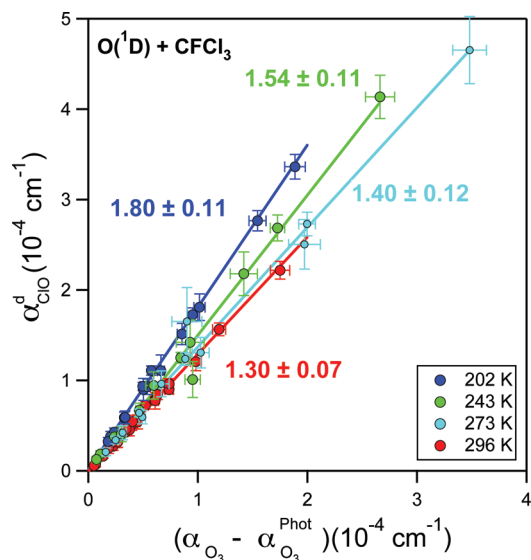


**Figure 7.** ClO radical product yield data obtained in this work for the O(<sup>1</sup>D) + CFCl<sub>3</sub> reaction at 202, 243, 273, and 296 K. The lines are linear least-squares fits to the data where the slope is proportional to  $Y_{\text{ClO}}\Delta\sigma_{\text{ClO}}$ , eq VII. The error bars are the  $2\sigma$  precision of the measurement.

consistency test for the  $\Delta\sigma_{\text{ClO}}(T)$  values obtained in our cross section determination experiments, which are used to obtain the absolute ClO product yields.

A summary of the room temperature ClO product yields obtained in this study and from previous studies is given in Table 1 and shown in Figure 8. Table 2 gives the results from this work for the ClO yield for the Cl<sub>2</sub> and CFCl<sub>3</sub> reactions as a function of temperature. The yields clearly show that ClO radical production is a major pathway in most of the reactions studied with values  $>0.7$  in many cases. None of the reactions, however, have a ClO yield  $>0.90$ , implying that other channels are active and collisional (physical) quenching of O(<sup>1</sup>D) to O(<sup>3</sup>P), reaction 1, is probably active in all of the reaction systems

studied. The lowest measured ClO yields were found for the HCl, CH<sub>3</sub>Cl, and CHF<sub>2</sub>Cl reactions where abstraction of the H atom to form an OH radical becomes a significant competing reaction pathway. The OH radical reaction product channels are  $\sim 20$ – $24$  kcal mol<sup>-1</sup> more exothermic than the ClO radical formation channels.

The precision of the ClO product yield measurements was on the order of 5–8% ( $2\sigma$ ) as shown in the examples given in Figure 7 and in the Supporting Information figures for the other species. The absolute ClO product yields were determined using  $\Delta\sigma_{\text{ClO}}(T)$  measured in this work where its estimated uncertainty is 10% at the  $2\sigma$  (95% confidence) level for all temperatures included in this study. The estimated overall uncertainty in the absolute ClO product yields are, therefore,  $\sim 13\%$  for each of the species included in this study. It is worth noting that the relative ClO product yields for these compounds were more accurately determined than the absolute values for the individual molecules.

**3.3. Comparison with Previous Studies.** There are several O(<sup>1</sup>D) reaction product yield studies with which to compare the present results. A summary of the results from previous studies, performed at room temperature, is given in Table 1. Overall, the agreement among the previous relative and indirect studies with the present absolute ClO reaction product yield results is good with a few exceptions. In the previous studies, O(<sup>1</sup>D) was produced by O<sub>3</sub> photolysis, as in the present study. The molecules studied and the detection methods used, however, varied as described briefly below.

Takahashi et al.<sup>9</sup> reported the most comprehensive study of ClO radical product yields for chloromethanes and chlorofluoromethanes to date. In fact, their study provided the only product yield data for several of these molecules prior to the present work. Our work includes all of the chloromethanes and chlorofluoromethanes studied by Takahashi et al. Takahashi et al.<sup>9</sup> used VUV-LIF detection of the ClO radical following the pulsed laser photolysis of O<sub>3</sub> at 248 nm in the presence of the chlorinated compounds. The uncalibrated ClO fluorescence signals obtained were scaled to the absolute ClO radical yield reported by Wine et al.<sup>24</sup> for the O(<sup>1</sup>D) + HCl reaction,  $0.24 \pm 0.05$ . The yield from the Wine et al. study was obtained from their measured H atom product branching ratio, ClO coproduct, and the quoted uncertainty is the  $2\sigma$  precision of their measurement. The large uncertainty in the reference reaction leads to correspondingly large uncertainties in the absolute ClO product yields reported by Takahashi et al. The agreement of the Takahashi et al.<sup>9</sup> ClO yields with the absolute measurements in the present study is, however, reasonable.

The trend in the ClO yield with increasing chlorination, replacing H atoms with Cl atoms, as shown in Figure 8 is somewhat different between this work and that of Takahashi et al.<sup>9</sup> Our results show a weak decrease in the ClO yield with decreasing chlorination between CCl<sub>4</sub> and CH<sub>2</sub>Cl<sub>2</sub>; the change is within the measurement uncertainty. Between CH<sub>2</sub>Cl<sub>2</sub> and CH<sub>3</sub>Cl we observe a significant decrease in the ClO yield. Takahashi et al.<sup>9</sup> report a nearly linear decrease in ClO yield with decreasing chlorination between CCl<sub>4</sub> and CH<sub>3</sub>Cl. The source of the discrepancy between our results and those of Takahashi et al.<sup>9</sup> is unknown. Measurement of the OH radical yield in these reactions, which are currently unavailable, would be useful to further investigate the trend in product channel yields.

There was no observed trend in the ClO yield with increasing fluorination, replacing Cl atoms with F atoms, between CFCl<sub>3</sub>, CF<sub>2</sub>Cl<sub>2</sub>, and CF<sub>3</sub>Cl. This result is in agreement with the results

**TABLE 1: Summary of ClO Product Yields Obtained in This Work in the O(<sup>1</sup>D) Reaction with Various Chlorine Containing Species and Comparison with Results from Previous Studies**

molecule	ClO Yield						
	this work <sup>a</sup>	Takahashi et al. <sup>9,b</sup>	Ravishankara et al. <sup>27,c</sup>	Wine et al. <sup>24,d</sup>	Wine et al. <sup>26,e</sup>	Force and Wiesenfeld <sup>28,f</sup>	Addison et al. <sup>25,g</sup>
Cl <sub>2</sub>	0.77 ± 0.10	0.74 ± 0.15			0.78 ± 0.17		
HCl	0.20 ± 0.04			0.24 ± 0.05			
CCl <sub>4</sub>	0.79 ± 0.04	0.90 ± 0.19				0.857 ± 0.093	
CHCl <sub>3</sub>	0.77 ± 0.04	0.71 ± 0.15					
CH <sub>2</sub> Cl <sub>2</sub>	0.73 ± 0.04	0.64 ± 0.13					
CH <sub>3</sub> Cl	0.46 ± 0.06	0.47 ± 0.10					
CFCl <sub>3</sub>	0.79 ± 0.04	0.88 ± 0.18				0.875 ± 0.084	0.65
CF <sub>2</sub> Cl <sub>2</sub>	0.76 ± 0.06	0.87 ± 0.18				0.857 ± 0.188	
CF <sub>3</sub> Cl	0.82 ± 0.06	0.85 ± 0.18	0.69 ± 0.10			0.491 ± 0.028	
CHFCl <sub>2</sub>	0.73 ± 0.05	0.74 ± 0.15					
CHF <sub>2</sub> Cl	0.56 ± 0.03						0.55 ± 0.10

<sup>a</sup> Quoted error limits are 2σ (95% confidence level) of the measurement precision. <sup>b</sup> ClO yield values scaled to the yield in the O(<sup>1</sup>D) + HCl reaction value reported by Wine et al.<sup>24</sup> <sup>c</sup> Indirect determination, obtained by difference from measured O(<sup>1</sup>D) collisional quenching branching ratio. <sup>d</sup> Indirect determination, taken as equal to the measured H atom product yield. <sup>e</sup> Indirect determination, obtained by difference from measured O(<sup>1</sup>D) collisional quenching branching ratio. <sup>f</sup> Indirect determination, obtained using deactivation rates of O(<sup>1</sup>D). <sup>g</sup> Measured using flash photolysis and photographic transient UV absorption of ClO radicals.

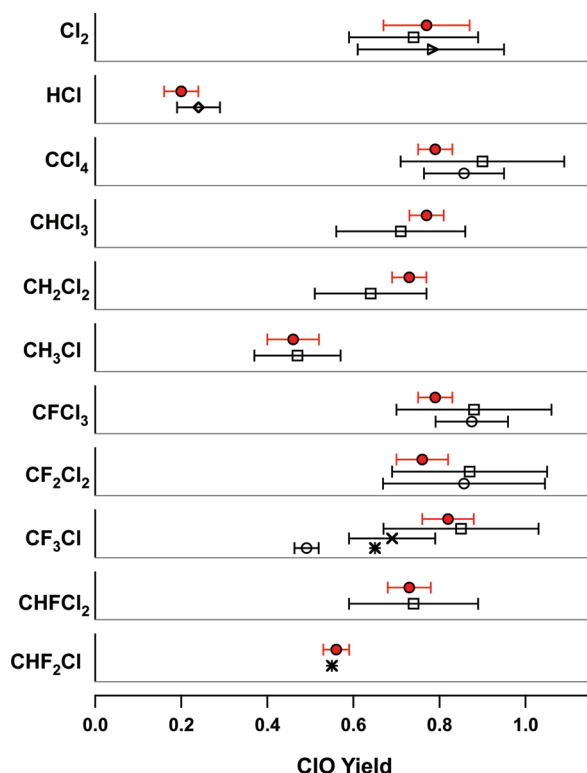


**Figure 8.** Summary of absolute ClO radical reaction product yields obtained in this work (●) at 296 K for the gas-phase O(<sup>1</sup>D) reaction with chlorine containing species. The error bars are at the 2σ (95% confidence) level. Results from previous studies are included for comparison: Takahashi et al.<sup>9</sup> (□); Ravishankara et al.<sup>27</sup> (×); Wine et al.<sup>24</sup> (Δ), Wine et al.<sup>26</sup> (◇); Force and Wiesenfeld<sup>28</sup> (○); Addison et al.<sup>25</sup> (\*). The data are also given in Table 1.

from Takahashi et al.<sup>9</sup> That is, although the overall rate coefficient of the O(<sup>1</sup>D) reaction decreases significantly with increasing fluorination, the relative ClO yield and collisional quenching terms remain nearly constant even though the number of available Cl atoms decreased. Significant decreases in the ClO yield was, however, observed between CF<sub>3</sub>Cl and CHFCl<sub>2</sub> and between CF<sub>2</sub>Cl<sub>2</sub> and CHF<sub>2</sub>Cl, presumably due to the opening of the OH radical product and reactive quenching channels.<sup>25</sup>

Addison et al.<sup>25</sup> studied the reaction of O(<sup>1</sup>D) with CF<sub>3</sub>Cl and CHF<sub>2</sub>Cl using photographic detection of ClO and CF<sub>2</sub> radical spectra in the UV/vis region combined with O atom and

**TABLE 2: Summary of ClO Product Yields for the O(<sup>1</sup>D) + Cl<sub>2</sub> and CFCl<sub>3</sub> Reactions as a Function of Temperature Obtained in This Work**

molecule	ClO Yield			
	296 K	273 K	243 K	202 K
Cl <sub>2</sub>	0.77 ± 0.10 <sup>a</sup>			0.77 ± 0.16
CFCl <sub>3</sub>	0.79 ± 0.04	0.79 ± 0.07	0.77 ± 0.06	0.75 ± 0.05

<sup>a</sup> Quoted error limits are 2σ (95% confidence level) of the measurement precision.

OH radical resonance absorption. For CHF<sub>2</sub>Cl, a significant yield for the reactive quenching HCl + CF<sub>2</sub> + O product channel, 45 ± 10%, was deduced primarily from the observed CF<sub>2</sub> radical formation. The formation of CF<sub>2</sub> as a reaction product implies a reaction mechanism involving the initial insertion of the O(<sup>1</sup>D) atom into the reactant molecule. A small OH radical yield of ~5% was also reported. A ClO product yield of 55% was reported, which is in good agreement with the present results. For CF<sub>3</sub>Cl, Addison et al.<sup>25</sup> report a ClO yield of 65%, which is significantly lower than the yield obtained in the present study.

Wine et al.<sup>26</sup> (Cl<sub>2</sub>), Wine et al.<sup>24</sup> (HCl), Ravishankara et al.<sup>27</sup> (CF<sub>3</sub>Cl), and Force and Wiesenfeld<sup>28</sup> (CCl<sub>4</sub>, CFCl<sub>3</sub>, CF<sub>2</sub>Cl<sub>2</sub>, and CF<sub>3</sub>Cl) reported ClO yields for the reactants in parentheses using pulsed laser photolysis of O<sub>3</sub> at 248 nm to produce O(<sup>1</sup>D). ClO radicals were not detected in these studies, but their yields were inferred from the Cl atom yield in the Cl<sub>2</sub> reaction, H atom yield in the HCl reaction, and collisional quenching branching ratio for the CCl<sub>4</sub>, CFCl<sub>3</sub>, CF<sub>2</sub>Cl<sub>2</sub>, and CF<sub>3</sub>Cl reactions assuming that ClO radical production was the only reactive pathway. Takahashi et al.,<sup>9</sup> however, reported a small, 5%, yield of Cl atoms in the O(<sup>1</sup>D) + CF<sub>3</sub>Cl reaction as a reactive quenching pathway that was not considered previously. The ClO radical yields reported in these studies are in general agreement with the present results, within their quoted error limits, with the exception of the value for CF<sub>3</sub>Cl reported by Force and Wiesenfeld.<sup>28</sup>

#### 4. Conclusion

In this study, absolute ClO radical product yields in the reaction of O(<sup>1</sup>D) with Cl<sub>2</sub>, HCl, CCl<sub>4</sub>, CHCl<sub>3</sub>, CH<sub>2</sub>Cl<sub>2</sub>, CH<sub>3</sub>Cl, CFCl<sub>3</sub>, CF<sub>2</sub>Cl<sub>2</sub>, CF<sub>3</sub>Cl, CHFCl<sub>2</sub>, and CHF<sub>2</sub>Cl are reported. ClO radical production was found to be a significant reaction pathway in the Cl<sub>2</sub>, CCl<sub>4</sub>, CHCl<sub>3</sub>, CH<sub>2</sub>Cl<sub>2</sub>, CFCl<sub>3</sub>, CF<sub>2</sub>Cl<sub>2</sub>, CF<sub>3</sub>Cl, and

CHFCl<sub>2</sub> reactions. Significantly lower ClO yields were found for the O(<sup>1</sup>D) reactions with HCl, CH<sub>3</sub>Cl, and CHF<sub>2</sub>Cl due most likely to the increased competition with the OH radical formation reaction pathway. The results obtained here are in good agreement with those obtained in previous relative and indirect determinations of ClO radical yields but more accurate. The ClO yields in the Cl<sub>2</sub> and CFCl<sub>3</sub> reactions were also examined over the temperature range 202–296 K and found to be independent of temperature within the precision of the measurements.

**Acknowledgment.** We thank R. Talukdar for help in designing of the reaction cell. This work was supported in part by NOAA's Climate Goal and NASA's Atmospheric Composition program.

**Supporting Information Available:** Figures of experimental ClO radical yield data for Cl<sub>2</sub>, HCl, CCl<sub>4</sub>, CHCl<sub>3</sub>, CH<sub>2</sub>Cl<sub>2</sub>, CH<sub>3</sub>Cl, CF<sub>2</sub>Cl<sub>2</sub>, CF<sub>3</sub>Cl, CHFCl<sub>2</sub>, and CHF<sub>2</sub>Cl. This material is available free of charge via the Internet at <http://pubs.acs.org>.

## References and Notes

- (1) *Scientific Assessment of ozone Depletion: 2006*; Global Ozone Research and Monitoring Project, WMO (World Meteorological Organization): Geneva, Switzerland, 2007.
- (2) Matsumi, Y.; Tonokura, K.; Kawasaki, M.; Tsuji, K.; Obi, K. *J. Chem. Phys.* **1993**, *98*, 8330.
- (3) Kohguchi, H.; Suzuki, T.; Nanbu, S.; Ishida, T.; Mil'nikov, G. V.; Oloyede, P.; Nakamura, H. *J. Phys. Chem. A* **2008**, *112*, 818.
- (4) Schinke, R. *J. Chem. Phys.* **1984**, *80*, 5510.
- (5) Yang, H.; Han, K. L.; Nanbu, S.; Nakamura, H.; Balint-Kurti, G. G.; Zhang, H.; Smith, S. C.; Hankel, M. *J. Phys. Chem. A* **2008**, *112*, 7947.
- (6) Bittererová, M.; Bowman, J. M.; Peterson, K. *J. Chem. Phys.* **2000**, *113*, 6186.
- (7) Matsumi, Y.; Shamsuddin, S. M. *J. Chem. Phys.* **1995**, *103*, 4490.
- (8) Sander, S. P.; Friedl, R. R.; Golden, D. M.; Kurylo, M. J.; Moortgat, G. K.; Keller-Rudek, H.; Wine, P. H.; Ravishankara, A. R.; Kolb, C. E.; Molina, M. J.; Finlayson-Pitts, B. J.; Huie, R. E.; Orkin, V. L. *Chemical kinetics and photochemical data for use in atmospheric studies*; JPL Pub. 06-2; Jet Propulsion Laboratory: Pasadena, CA, U.S., 2006; Evaluation Number 15.
- (9) Takahashi, K.; Wada, R.; Matsumi, Y.; Kawasaki, M. *J. Phys. Chem.* **1996**, *100*, 10145.
- (10) O'Keefe, A.; Deacon, D. A. G. *Rev. Sci. Instrum.* **1988**, *59*, 2544.
- (11) Yalin, A. P.; Zare, R. N. *Laser Phys.* **2002**, *12*, 1065.
- (12) Gierczak, T.; Rajakumar, B.; Flad, J. E.; Burkholder, J. B. *Int. J. Chem. Kinet.* **2009**, *41*, 543.
- (13) Gierczak, T.; Rajakumar, B.; Flad, J. E.; Burkholder, J. B. *Chem. Phys. Lett.* **2010**, *484*, 160.
- (14) Rajakumar, B.; Flad, J. E.; Gierczak, T.; Ravishankara, A. R.; Burkholder, J. B. *J. Phys. Chem. A* **2007**, *111*, 8950.
- (15) Rajakumar, B.; Gierczak, T.; Flad, J. E.; Ravishankara, A. R.; Burkholder, J. B. *J. Photochem. Photobiol., A: Chem.* **2008**, *199*, 336.
- (16) Zou, P.; Shu, J.; North, S. W. *J. Photochem. Photobiol., A: Chem.* **2010**, *209*, 56.
- (17) McPheat, R.; Duxbury, G. *J. Quant. Spectrosc. Radiat. Transfer* **2000**, *66*, 153.
- (18) Nemtchinov, V.; Varanasi, P. *J. Quant. Spectrosc. Radiat. Transfer* **2003**, *82*, 473.
- (19) Orkin, V. L.; Guschin, A. G.; Larin, I. K.; Huie, R. E.; Kurylo, M. J. *J. Photochem. Photobiol., A: Chem.* **2003**, *157*, 211.
- (20) Varanasi, P.; Chudamani, S. *J. Geophys. Res.* **1988**, *93*, 1666.
- (21) Wang, Y.; Tremmel, J.; Smedt, J. D.; Alsenoy, C. V.; Geise, H. J.; Van der Veken, B. *J. Phys. Chem. A* **1997**, *101*, 5919.
- (22) McLoughlin, P. W.; Park, C. R.; Wiesenfeld, J. R. *J. Mol. Spectrosc.* **1993**, *162*, 307.
- (23) Barton, S. A.; Coxon, J. A.; Roychowdhury, U. K. *Can. J. Phys.* **1984**, *62*, 473.
- (24) Wine, P. H.; Wells, J. R.; Ravishankara, A. R. *J. Chem. Phys.* **1986**, *84*, 1349.
- (25) Addison, M. C.; Donovan, R. J.; Garraway, J. *Faraday Discuss. Chem. Soc.* **1979**, *67*, 286.
- (26) Wine, P. H.; Nicovich, J. M.; Ravishankara, A. R. *J. Phys. Chem.* **1985**, *89*, 3914.
- (27) Ravishankara, A. R.; Solomon, S.; Turnipseed, A. A.; Warren, R. F. *Science* **1993**, *259*, 194.
- (28) Force, A. P.; Wiesenfeld, J. R. *J. Phys. Chem.* **1981**, *85*, 782.

JP107761T